Facile synthesis of mesoporous VO_2 nanocrystals by a cotton-template method and their enhanced thermochromic properties

Shaowen Wu [a], Shouqin Tian [a,b,*] , Baoshun Liu [a], Haizheng Tao [a], Xiujian Zhao [a,*], R. G. Palgrave [b], G. Sankar [b] and I.P. Parkin[b]

[a] State Key Laboratory of Silicate Materials for Architectures, Wuhan University of Technology (WUT), No. 122, Luoshi Road, Wuhan 430070, P. R. China

[b] Department of Chemistry, Materials Chemistry Centre, University College London, 20 Gordon St., London WC1H 0AJ, UK

*Corresponding author. Tel.: +86-027-87652553; Fax: +86-027-87883743.

E-mail address: tiansq@whut.edu.cn (S. Tian); opluse@whut.edu.cn (X. Zhao)

Abstract:

As a very promising thermochromic material, VO_2 (M/R) (Monoclinic/Rutile) has not been widely applied in smart windows due to its intrinsic low solar modulation (ΔT_{sol}) and low luminous transmission (T_{lum}). To address this issue, porous structures have been introduced into the VO_2 film. Herein, mesoporous VO_2 powders with pore size of about 2～10 nm were synthesized using cotton as template by hydrothermal methods. The pore and crystal size of the synthesized VO_2 powders can be reliably controlled by the hydrothermal temperature. The mesoporous VO_2 powders were mixed with PVP to prepare the VO_2-based nanocomposite films by spin coating. The VO_2-based films show a better performance between ΔT_{sol} and T_{lum} than that appeared in previous reports. Especially, a larger pore size could lead to a higher visible transmittance and a larger crystal size would facilitate the enhancement in the solar modulation. In this sense, the VO_2-based film obtained at the hydrothermal temperature of 180 ℃ exhibits an outstanding thermochromic performance with ΔT_{sol} of 12.9% and T_{lum} up to 56.0% due to the larger crystal and pore sizes. Therefore, this synthetic route shows a potential method for the application of mesoporous VO_2 powders for solar control coatings.

Keywords: VO_2 film; mesoporous structure; thermochromic property; solar modulation ability;

1. Introduction

Monoclinic/rutile (M/R)-phase vanadium dioxide (VO_2) undergoes a fully reversible metal-semiconductor transition (MST) at a critical temperature (T_c) of *ca*. 68 ℃ [1]. This phase transition results in dramatic changes in the optical and electrical properties [2-3]. Below the T_c, VO_2 displays monoclinic crystal structure, which is transparent to near-infrared light due to semiconducting property. Above the T_c, VO_2 displays the rutile crystal structure and is highly reflective to near infrared light while maintaining visible-light transparency due to semi-metallic property. This property could make VO_2 a promising material for smart windows [4]. However, thin films of VO_2 suffer from poor visible light transmission due to strong inner-band absorptions for both the metallic and semiconducting states [1]. In addition, the low solar modulation (ΔT_{sol}) of VO_2 also limits its application. To date, a number of chemical and physical approaches have been employed to improve luminous transmission while maintaining high solar modulation, including film thickness optimization [5], doping [6,7], multilayer-stack design [8], introducing pores [9,10] and the formation of composite films [11]. Optical calculations suggest that VO_2 nanoparticles dispersed in a dielectric host are more advantageous than VO_2 continuous thin solid films in smart window applications [12] because they can offer much higher luminous transmission (T_{lum}) and enhanced ΔT_{sol}. Liu *et al* [13] prepared the composite films with VO_2 powders dispersed in Si-Al composite sol. The T_{lum} and ΔT_{sol} of these composite film reached 61% and 12%, respectively. Gao *et al* [14] prepared composite films with VO_2@SiO_2 powders dispersed in aqueous solution containing polyurethane (PU). In this study, it is shown that the visible transparence and solar modulation ability of the VO_2 films can be enhanced by the addition of the PVP resulting in a composite. Therefore, VO_2 nanoparticles distributed in another dielectric matrix can offer a novel perspective to achieve high values for T_{lum} and ΔT_{sol}.

Inspired by this concept, we report here the synthesis of highly porous VO_2(M) films . Xie *et al* prepared a periodic porous thermochromic VO_2(M) film [10]. The two-dimensional periodic porous VO_2(M) film exhibited high T_{lum} (81% maximum). However, the solar modulation ability was only 7.9% due to the large pore size (~ 200 nm). Kang *et al* [12] employed polymer-assisted deposition technique to obtain a nanoporous film with an average pore size of ~28 nm, which

exhibited a high ΔT_{sol} of 14.1%. The value of T_{lum}, however, was only 41% probably because of the small pores. In this regard, it is still a challenge to control the pore size in the VO_2 film to obtain a good balance between visible transparency and solar modulation. Especially, most works are focused on the pore size between VO_2 nanoparticles in the film. However, the effect of pore size in the VO_2 nanocrystals on the thermochromic properties of films based on the VO_2 nanocrystals has been not been reported so far, to our knowledge. Therefore, it is of great importance to investigate the effect of pore size in the VO_2 nanocrystals on the thermochromic properties of VO_2 films consisted of nanocrystals.

In this work, porous VO_2 nanocrystals with 2~10 nm in pore size have been prepared by a facile hydrothermal method using cotton as a template. A post heat treatment under ammonium bicarbonate (NH_4HCO_4) gas yields porous VO_2 powders. The crystallinity and pore size of the VO_2 nanocrystals appears to be controllable through the hydrothermal reaction temperature. Spin coated thin films from the VO_2 powders exhibit a good balance between visible transparence (T_{lum} = 56.0%) and solar modulation ability (ΔT_{sol} = 12.9%) due to the introduction of the porous structure and creating a composite with PVP in the film preparation stage.

2. Experiments and characterization

2.1 Preparation of mesoporous VO_2 nanoparticles

All reagents were purchased from the Sinopharm Chemical Reagent Co., Ltd., and were used without further purification. 0.4 g (0.0022 mol) of vanadium pentoxide (V_2O_5) and 0.832 g (0.0066 mol) of oxalic acid were dissolved in 30 ml of water, and then 30 ml of ethylene glycol was added to increase the viscosity of the solution. As the cotton degrades the acidic solutions, 1 ml of ammonia was added to adjust the pH to *ca*. 7. The solution and 0.3 g of cotton were transferred to a 100 mL Teflon-lined stainless-steel autoclave. The autoclave was maintained at a temperature of 180 ℃ for 20 h and then cooled to room temperature naturally. The black product was separated and washed with water and ethanol, and then dried in air at 80 ℃ for 24 h. In order to remove the template to get porous powders, the product was heated, in air, at 400 ℃ for 1 h, ramp rate *ca*. 3 ℃ min^{-1}. As comparison, samples were also prepared at hydrothermal temperature of 120 ℃, 140 ℃ and 160 ℃ which are denoted as Sample a, Sample b and Sample

c; the sample prepared at hydrothermal temperature of 180oC is denoted as sample d. Finally, 0.2 g of the obtained mesoporous V_2O_5 and 0.1 g of NH_4HCO_4 were placed in a vacuum tube furnace for 450 ℃ for 30 min. Ammonia produced from the decomposition of NH_4HCO_4 reduced V_2O_5 to VO_2

Preparation of Films

0.5 g of VO_2 nanoparticles were dispersed in ethanol that contained 0.25 g of PVP by grinding. This solution was then sonicated to ensure good mixing. After centrifugation at 8000 rpm, a suspension was formed. This suspension was then uniformly cast onto a float glass substrate by spin-coating at the speed of 500 rpm for 10 s and then 1000 rpm for 20 s. Finally the ethanol was removed by drying in an oven at 80 °C for 1 min, yielding VO_2-based composite films.

2.2 Characterization

The crystalline phases of the nanoparticles in the powder form, were determined by X-ray diffraction (XRD, D8Advance, CuKα, λ = 0.154178 nm produced under a 3 kW output power). The morphologies of the powders and films were examined by a field emission scanning electron microscopy (SEM, JSM-5610LV, Japan) and field emission transmission electron microscopy (TEM, JEM2100, Japan). Pore size and distribution of the powders was determined by nitrogen adsorption–desorption using a BET analyzer. The compositions of the powders were determined by X-ray photoelectron spectroscopy (XPS). The thermochromic properties of the films from 300 to 2500 nm was measured with ultraviolet–visible–near-infrared spectrophotometer (UV–Vis–NIR, UV-3600) at temperature 20 and 90 ℃, respectively.

The integrated luminous transmittance (T_{lum}, 380-780 nm) and solar transmittance (T_{sol}, 300−2500 nm) were obtained from the following equation [15]

$$T_{lum/sol} = \int \varphi_{lum/sol}(\lambda) T(\lambda) d\lambda / \int \varphi_{lum/sol}(\lambda) d\lambda$$

Where, T(λ) denotes film transmittance at wavelength λ, $\varphi_{lum}(\lambda)$ is the standard luminous efficiency function for the photopic vision of human eyes, $\varphi_{sol}(\lambda)$ is the solar irradiance spectrum for air mass 1.5 corresponding to the sun standing 37° above the horizon. ΔT_{sol} is attained from $\Delta T_{sol} = T_{sol}$ (20 ℃) -T_{sol} (90 ℃).

3. Results and discussion

3.1 The structure of VO_2 nanocrystals

The XRD patterns of the powder samples obtained by annealing the V_2O_5 in an ammonia atmosphere at 400 ℃ and 450 ℃ for 30 min are shown in Fig. 1. In addition to the diffraction peaks corresponding to M-phase VO_2 (JCPDS card no.44-252), additional reflections due to V_6O_{13} (JCPDS card no.71-2235) phase were also seen for samples annealed at 400 °C. Only the M-phase VO_2 was detected when the annealing temperature was raised to 450 ℃. This suggests that there is an energy barrier that needs to be overcome to obtain M-phase VO_2.

In order to determine the morphology of the samples synthesized, SEM images of the sample d (produced from hydrothermal reaction at 180oC and subsequently reduced at 450oC) are shown in Fig. 2(a, b). It can be seen from Fig. 2(a) that the samples have a fibrous morphology. The diameter of the VO_2 fibers was estimated to be 5-10 μm. Interestingly, the VO_2 fibers consisted of clusters of small nanoparticles with pores present between the particles is seen in an enlarged image which is shown in Fig. 2(b). Further enlarged TEM images of the same sample, shown in Fig. 2(c), show that the samples are clusters of nanoparticles with a diameter *ca*. 100 nm, with mesopores present between the nanoparticles. This supports the morphology observed in the SEM images, Fig. 2(b). In Fig. 2(d), the lattice planes are clearly seen, these give an interplanar spacing of d = 0.320 nm corresponding to the (011) plane of monoclinic VO_2. This is consistent with the XRD results. In addition, the clear lattice fringe indicated good crystallinity of the synthesized VO_2.

In order to examine the oxidation states of the vanadium in the synthesized VO_2 powders, XPS measurements were performed and the results are shown in Fig. 3. The full spectra in Fig. 3(a) suggests the presence of oxygen and vanadium in the samples. C1s is used as reference. As can be seen from Fig. 3(b), the samples contain two vanadium oxidation states, which correspond to V^{5+} and V^{4+}, at a binding energy of 517.0 eV and 515.6 eV, respectively [16]. The presence of V^{5+} ions could be attributed to the partial surface oxidation of the samples exposed in air. In addition, the energy gap between O1s and $V2p_{3/2}$ is 14.0 eV, which is in good agreement with the value of 14.2 eV in the previous work [17]. In this sense, the results indicate that the obtained

sample is pure VO_2.

In order to further investigate the porous structures of the powder samples, BET characterization was employed and the results are shown in Fig. 4. As can be seen from N_2 adsorption/desorption curves in Fig. 4, the adsorption isotherm displays type Ⅳbehavior with H3 hysteresis loops, indicating slit-shaped mesopores [18]. In addition, the adsorption capacity is increased with an increase of p/p_0 across the whole pressure range, indicating that there are abundant mesopores in the samples. The pore size distribution curves show that the distribution of pores in the samples is narrow and the typical pore size in the range of ca 2～10 nm. In addition, there is a second set of pores in the size range of 10～50 nm.

3.2 The thermochromic characteristics of VO_2-based composite films

To investigate the thermochromic properties, thin films of the porous VO_2 powders were deposited by spin-coating a suspension containing PVP and the powder onto float glass. As can be seen from Fig. 5(a), the VO_2 composite films are homogeneous, transparent, and light brownish- yellow in colour. As shown in Fig. 5(b), the thickness of the film is about 628 nm, which are much smaller than that of the composite films prepared in other previous works [13,19], thus leading to a high visible light transmittance. Uniform dispersion of powders into thin films has been shown to have an important effect on enhancing the thermochromic properties of the deposited film [20]. Therefore, in order to further understand the distribution of the VO_2 powders in the film, the distribution of the O and V element in the film was investigated by elemental mapping methods. It is clear from Fig. 5(c) and (d) that both O and V elements are distributed uniformly in the film without agglomeration, indicating that the powders are homogeneously dispersed in the film.

To further investigate the thermochromic properties, variable temperature UV-Vis–NIR transmittance spectra were obtained. The optical transmittance spectra for Sample d are shown in Fig. 6. It can be clearly seen that the PVP-VO_2-composite films exhibited excellent optical properties, with high visible light transmittance. It reaches a sufficiently high visible transmission (T_{lum}) of 56.0% and still retains an excellent solar modulating ability (ΔT_{sol}) of 12.9%, which are better than that reported for the pure VO_2 films [21] and even TiO_2 /VO_2 /TiO_2

/VO_2 /TiO_2 five-layered film [22]. These results are quite encouraging, especially for the practical application in solar control coatings.

3.3 The effect of hydrothermal temperature on structure and properties of VO_2 powders

In order to investigate the effect of hydrothermal temperature on the crystallinity and pore size of VO_2 nanocrystals, 120 ℃, 140 ℃ and 160 ℃, which are denoted as Sample a, Sample b and Sample c, respectively and were chosen as comparison to the Sample d prepared at 180oC. As shown in Fig. 7, all the diffraction peaks in the XRD patterns belong to M-phase VO_2 (JCPDS card no.44-252), indicating that the four samples are pure VO_2. Increasing the hydrothermal temperature leads to an increase in the XRD peak intensity of the samples. This suggests that the crystallinity of the samples becomes higher with increasing temperature and thus Sample d exhibit the highest crystallinity. The grain size of Sample a, b, c, d calculated by the Scherrer equation are 36.2 nm, 36.3 nm, 59.4 nm, 60.7 nm, respectively. This indicates that the samples prepared at higher hydrothermal temperature show a larger crystallite size and thus Sample d exhibited the largest crystallite size.

SEM images for Sample a, Sample b, Sample c and Sample d are shown in Fig. 8. It can be clearly seen that these four samples keep the morphology of cotton and show the same porous structures as observed for the sample shown in Fig 2. Sample a and Sample b are more agglomerated than Sample c and Sample d, with fewer pores observable in the microstructure. This is attributed to the preparation process for Sample a and sample b. It is also found that there is poor adhesion between the nanocrystals and the absorbent cotton prepared at 120 ℃ and 140 ℃, which means that these samples could not be sufficiently washed and the ethylene glycol is not completely removed by the washing procedure. During the later heating process, the residual ethylene glycol causes the powders to agglomerate and grow. Larger agglomerated particles would affect the transmittance of the film. As can be seen in Fig. 8(c) and (d), Sample c and Sample d show a more obvious porosity and clearer particle interface, which means that the particles are more easily dispersed. In addition, the particle size of Sample d is larger than Sample c, indicating that a higher hydrothermal temperature leads to a larger particle size. This is in good agreement with the values shown from the Scherer analysis of the XRD results.

The corresponding N_2 adsorption/desorption and pore size distribution curves of Sample a, b, c and d are shown in Fig. 9. It can be clearly seen that the adsorption isotherms of all samples display type Ⅳ behavior with H3 hysteresis loops. The estimated mean pore size is 3.23 nm, 5.05 nm, 10.58 nm and 3.78 nm for Sample a, Sample b, Sample c and Sample d, respectively. This indicates that the pore size is increased at first and then decreased with increasing the hydrothermal temperature from 120 to 180 °C. Also, Sample c exhibits the largest pore size than other three samples. This is related with the formation of pores in the samples. The pores are produced by the combustion of the cotton and caused by aggregates of nanoparticles. In this sense, a larger crystallite size of the sample prepared at higher hydrothermal temperature could lead to larger pore size [23] so that the order of samples in pore size is presented as follows: Sample a < Sample b < Sample c. However, Sample d with a larger crystalline size exhibits a smaller pore size. This is probably because that the degree crystallinity of Sample d has increased and less cotton remains in the product due to the dissolution of cotton in the solution at the hydrothermal temperature of 180 °C. The large pore size of VO_2 powders would lead to the enhancement in the visible light transmittance of VO_2 films.

Variable temperature UV/vis spectra of thin films of Sample a, b, c, d are shown in Fig. 10. It can be clearly seen that the transmittance of composite films changed with the temperature of the hydrothermal treatment, with higher temperatures leading to greater visible light transmission. The optical properties of VO_2 composite films are summarized in Table 1. Upon increasing the hydrothermal temperature from 120 ℃ to 160 ℃, T_{lum} is increased from 50.1% to 59.0 %. At a hydrothermal treatment temperature of 180 °C, there is a decrease to 56.0% in the T_{lum}. The reason for the visible transmittance reaching a maximum (59.0%) for Sample c is probably due to the largest pore size. This can facilitate the uniform dispersion of nanocrystals in the PVP for enhanced visible transmittance. In this paper, PVP was selected as the matrix, not only because it is highly transparent, but it can modify the surface of the nanoparticles to improve the dispersion of nanoparticles [13]. In this sense, the mesoporous structure of the powders also plays a critical role in regulating the visible light transmittance of the film. When the hydrothermal temperature is increased, the solar modulation value of ΔT_{sol} is increased from 9.8% to 12.9%. Also, the

crystallinity and particle size of the VO_2 nanoparticles are also increased with an increase in the hydrothermal temperature. It can be clearly seen that the ΔT_{sol} of the VO_2-based film depends mainly on the crystallinity and particle size of the VO_2 nanoparticles in Table 1. Sample d shows the highest crystallinity and largest particle size, and thus its ΔT_{sol} is the highest (12.9%). Therefore, our composite films based on the mesoporous VO_2 powders exhibit much higher T_{lum} (56.0%) and ΔT_{sol} (12.9%) than VO_2-$BaSO_4$ composite films (T_{lum} = 43.5%, ΔT_{sol} = 12.4%) [24] and some VO_2-Sb:SnO_2 composite films (T_{lum} = 49.8%, ΔT_{sol} = 11.7%) [25].

4. Conclusion

In this work, mesoporous VO_2 nanocrystals with pore size of about 2～10 nm were synthesized by hydrothermal method at temperatures between 120 to 180 ℃and then coated into the float glass substrate as PVI-VO2 composite film. The VO_2 based film exhibits excellent thermochromic properties: a high visible transmittance of T_{lum} = 56.0% and a high solar modulating ability of ΔT_{sol} = 12.9%. In addition, the temperature of the hydrothermal treatment influences both the crystallinity and particle size of samples, and thus their thermochromic properties. The crystallinity of the nanocrystals prepared at 120 ℃ and 140 ℃ is poor and also suffers from a high degree of agglomeration of the particles, reducing the visible light transmittance and solar modulation. The crystallinity and dispersion of the powders prepared at 160 ℃ and 180 ℃ are better than those prepared at 120 ℃ and 140 ℃, with the composite film prepared by this method at 160 ℃ and 180 ℃ exhibits high visible transmittances of T_{lum} = 59.0%, 56.0% and high solar modulating abilities of ΔT_{sol} = 11.4%, 12.9%, respectively. Therefore, the synthetic route described has great potential to be applied in solar control coatings of thermochromic VO_2. .

Acknowledgements: This work was financially supported by NSFC (Nos. 51461135004, 51402225 and 51372180), NSF of Hubei Province (No. 2013CFA008), Doctoral Fund of Ministry of education priority development projects (No. 20130143130002), the Key Technology Innovation Project of Hubei Province (No. 2013AEA005) and EPSRC, ICE Glazing Project (EP/M003353/1).

References

[1] S. Wang, M. Liu, L. Kong, Y. Long, X. Jiang, A. Yu, Recent progress in VO_2 smart coatings: Strategies to improve the thermochromic properties, Prog. Mater. Sci. 81 (2016) 1-54.

[2] C. Wu, F. Feng, Y. Xie, Design of vanadium oxide structures with controllable electrical properties for energy applications, Chem. Soc. Rev. 42 (2013) 5157-5183.

[3] Y. Gao, H. Luo, Z. Zhang, L. Kang, Z. Chen, J. Du, M. Kanehire, C. Cao, Nanoceramic VO_2 thermochromic smart glass: a review on progress in solution processing, Nano Energy 1 (2012) 221–246.

[4] Malara F, Cannavale A, Carallo S, Gigli G. Smart windows for building integration: a new architecture for photovoltachromic devices, ACS Appl Mater Interfaces 6 (2014) 9290-9297.

[5] D. Malarde, M.J. Powell, R. Quesada-Cabrera, R.L. Wilson, C.J. Carmalt, G. Sankar, I.P. Parkin, R.G. Palgrave, Optimized atmospheric-pressure chemical vapor deposition thermochromic VO_2 thin films for intelligent window applications, ACS Omega 2 (2017) 1040−1046.

[6] J. D. Zhou, Y.F. Gao, X.L. Liu, Z. Chen, L. Dai, C.X. Cao, H.J. Luo, M. Kanahira, C. Sun, L. M. Yan, Mg-doped VO_2 nanoparticles: hydrothermal synthesis, enhanced visible transmittance and decreased metal-insulator transition temperature, Phys. Chem. Chem. Phys. 15 (2013) 7505−7511.

[7] S. Chen, L. Dai, J. J. Liu, Y.F. Gao, X.L. Liu, Z. Chen, J.D. Zhou, C.X. Cao, P.G. Han, H.J. Luo, M. Kanahira, The visible transmittance and solar modulation ability of VO_2 flexible foils simultaneously improved by Ti doping: an optimization and first principle study, Phys. Chem.

Chem. Phys. 15 (2013) 17537−17543.

[8] M.J. Powell, R. Quesada-Cabrera, A. Taylor, D. Teixeira, I. Papakonstantinou, R.G. Palgrave, G. Sankar, I.P. Parkin, Intelligent multifunctional $VO_2/SiO_2/TiO_2$ coatings for self-cleaning, energy-saving window panels, Chem. Mater. 28 (2016) 1369−1376.

[9] X. Cao, N. Wang, J. Y. Law, S. C. J. Loo, S. Magdassi, Y. Long, Nanoporous thermochromic VO_2 (M) thin films: controlled porosity, largely enhanced luminous transmittance and solar modulating ability, Langmuir 30 (2014) 1710–1715.

[10] M. Zhou, J. Bao, M. Tao, R. Zhu, Y. Lin, X. Zhang, Y. Xie, Periodic porous thermochromic VO_2(M) films with enhanced visible transmittance, Chem. Commun. 49 (2013) 6021-6023.

[11] J. Zhu, A. Huang, H. Ma, Y. Ma, K. Tong, S. Ji, S. Bao, X. Cao, P. Jin, Composite film of vanadium dioxide nanoparticles and ionic liquid−nickel−chlorine complexes with excellent visible thermochromic performance, ACS Appl. Mater. Interfaces 8 (2016) 29742−29748.

[12] L. Kang, Y. Gao, H. Luo, Z. Chen, J. Du, Z. Zhang, Nanoporous thermochromic VO_2 films with low optical constants, enhanced luminous transmittance and thermochromic properties, ACS Appl. Mater. Interfaces 3 (2011) 135–138.

[13] C. Liu, X. Cao, A. Kamyshny, J. Y. Law, S. Magdassi, Y. Long, VO_2/Si–Al gel nanocomposite thermochromic smart foils: largely enhanced luminous transmittance and solar modulation, J. Colloid Inter Sci. 427 (2014) 49-53.

[14] Y. Gao, S. Wang, H. Luo, L. Dai, C. Cao, Y. Liu, Z. Chen, M. Kanehira, Enhanced chemical stability of VO_2 nanoparticles by the formation of SiO_2/VO_2 core/shell structures and the application to transparent and flexible VO_2-based composite foils with excellent thermochromic

properties for solar heat control, Energy Environ. Sci. 5 **(**2012) 6104-6110.

[15] Q. Lu, C. Liu, N. Wang, Periodic micro-patterned VO_2 thermochromic films by mesh printing, J. Mater. Chem. C 4 (2016) 8385-8391.

[16] G. Silversmit, D. Depla, H. Poelman, G. B. Marin, R.D. Gryse, Determination of the V 2p XPS binding energies for different vanadium oxidation states (V^{5+} to V^{0+}), J. Electron Spectrosc. 135 (2004) 167–175.

[17] S.D. Ji, F. Zhang, P. Jin, Preparation of high performance pure single phase VO_2 nanopowder by hydrothermally reducing the V_2O_5 gel, Sol. Energy Mater. Sol. Cells 95 (2011) 3520–3526

[18] M.W. Xue, H. Chen, J.Z. Ge, J.Y. Shen, Preparation and characterization of thermally stable high surface area mesoporous vanadium oxides, Micropor. Mesopor. Mat. 131 (2010) 37–44.

[19] Z. Chen, Y.F. Gao, L.T. Kang, C.X. Cao, S. Chen, H.J. Luo, Fine crystalline VO_2 nanoparticles: synthesis, abnormal phase transition temperatures and excellent optical properties of a derived VO_2 nanocomposite foil, J. Mater. Chem. A, 2 (2014) 2718–2727.

[20] J.T. Zhu, Y.J. Zhou, B.B. Wang, J.Y. Zheng, S.D. Ji, H.L. Yao, H.J. Luo, P. Jin, Vanadium dioxide nanoparticle-based thermochromic smart coating: high luminous transmittance, excellent solar regulation efficiency, and near room temperature phase transition, ACS Appl. Mater. Interfaces 7 (2015) 27796−27803.

[21] Z. Chen, Y.F. Gao, L.T. Kang, J. Du, Z.T. Zhang, H.J. Luo, H.Y. Miao, G.Q. Tan, VO_2-based double-layered films for smart windows: optical design, all-solution preparation and improved properties, Sol. Energy Mater. Sol. Cells 95 (2011) 2677-2684.

[22] N.R. Mlyuka, G.A. Niklasson, C.G. Granqvist, Thermochromic multilayer films of VO_2 and TiO_2 with enhanced transmittance, Sol. Energy Mater. Sol. Cells 93 (2009) 1685-1687.

[23] S. Tian, X. Ding, D. Zeng, S. Zhang, C. Xie, Pore-size-dependent sensing property of hierarchical SnO_2 mesoporous microfibers as formaldehyde sensors, Sens. Actuators B 186 (2013) 640-647.

[24] W. Li , S. Ji, K. Qian, P. Jin, Preparation and characterization of VO_2–$BaSO_4$ composite films with enhanced optical properties in thermochromic field, Ceram. Int. 41 (2015) 5049–5056.

[25] W. Li, S. Ji, K. Qian, P. Jin, Preparation and characterization of VO_2 (M)–SnO_2 thermochromic films for application as energy-saving smart coatings, J. Colloid Interface Sci. 456 (2015) 166–173.

Figure captions:

Fig. 1 XRD patterns of VO_2 sample obtained by annealing V_2O_5 in an ammonia atmosphere at 400 ℃ and 450 ℃ for 30 min.

Fig. 2 (a) Low- and (b) high-magnification SEM, (c) TEM and (d) HRTEM images of the obtained sample.

Fig. 3 (a) Full XPS spectrum, (b) high resolution V 2p and O1s spectra of the obtained sample.

Fig. 4 N_2 adsorption/desorption curves and pore size distribution curves of the obtained sample.

Fig. 5 (a) the surface (the inset shows the photograph (2.5*2.5 cm) of film on the glass), (b) the cross-section SEM images, (c) O element distribution and (d) V element distributions of the VO_2 based film.

Fig. 6 Transmittance spectra of the films based on the VO_2 mesoporous particles at different temperatures.

Fig. 7 The XRD patterns of the samples prepared at different temperatures (a-120 ℃, b-140 ℃, c-160 ℃, d-180 ℃).

Fig. 8 SEM images of samples prepared at different temperatures (a) Sample a-120 ℃, (b) Sample b-140 ℃, (c) Sample c160 ℃ and (d) Sample d180 ℃.

Fig. 9 N_2 adsorption/desorption curves and pore size distribution curves of Samples prepared at different temperatures (a-120 ℃, b-140 ℃, c-160 ℃, d-180 ℃).

Fig. 10 Variable temperature UV/vis spectra of thin films of Samples prepared at different temperatures (a-120 ℃, b-140 ℃, c-160 ℃, d-180 ℃). The spectra were obtained at 20 and 90 °C.

Table captions:

Table 1 The thermochromic properties of VO_2 composite films at different hydrothermal temperatures.

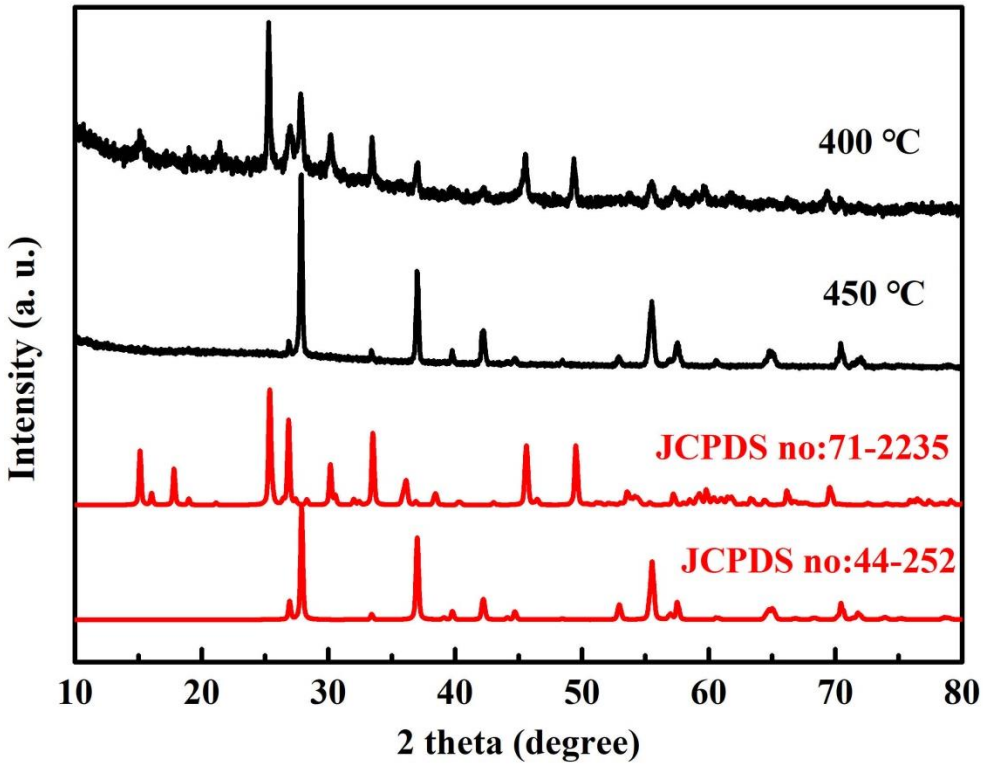

Fig. 1 XRD patterns of Sample d (prepared at 180oC hydrothermal reaction temperature) obtained by annealing V_2O_5 in an ammonia atmosphere at 400 ℃ and 450 ℃ for 30 min.

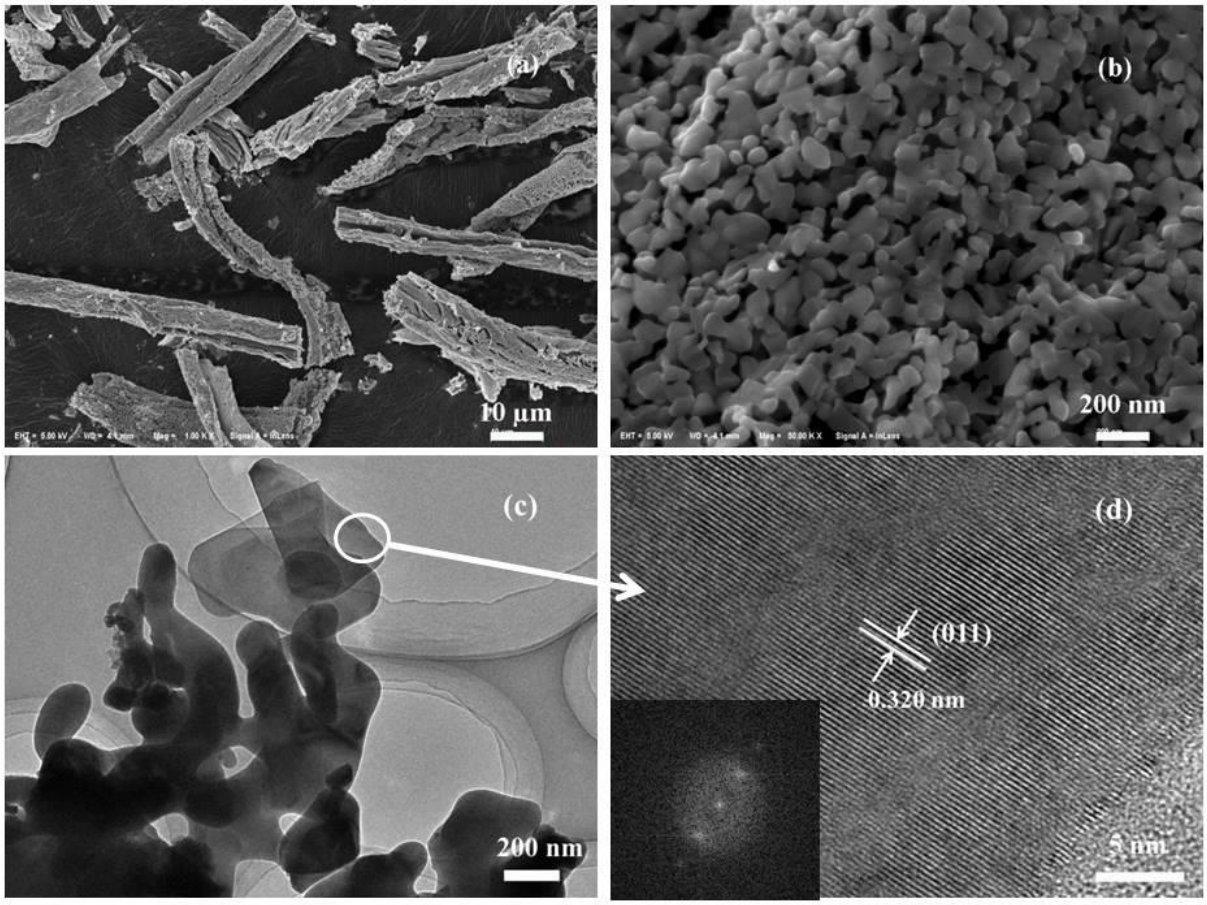

Fig. 2 (a) Low- and (b) high-magnification SEM, (c) TEM and (d) HRTEM images of the VO2 sample prepared from the Sample d produced at 180oC hydrothermal reaction temperature.

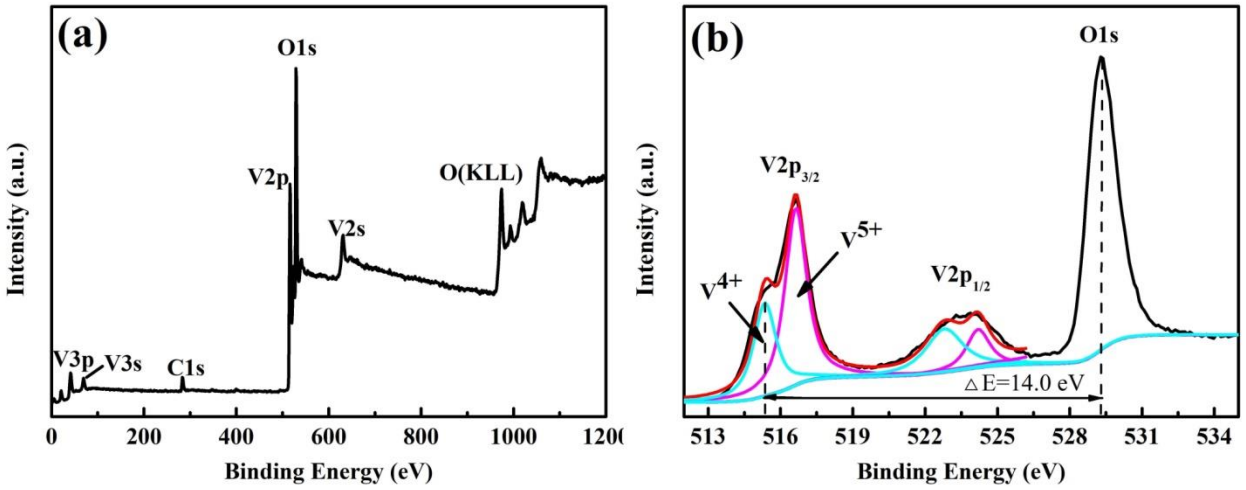

Fig. 3 (a) Full XPS spectrum, (b) high resolution V 2p and O1s spectra of the VO2 sample prepared from the Sample d produced at 180oC hydrothermal reaction temperature.

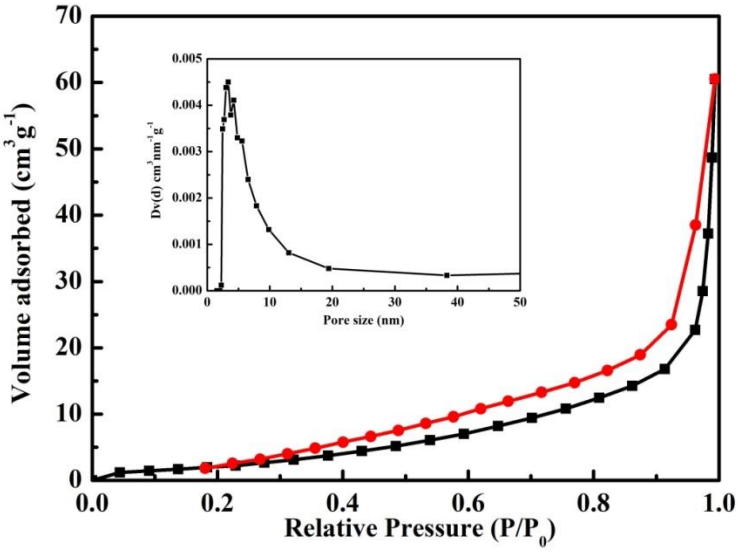

Fig. 4 N_2 adsorption/desorption curves and pore size distribution curves of the VO2 sample prepared from the Sample d produced at 180oC hydrothermal reaction temperature.

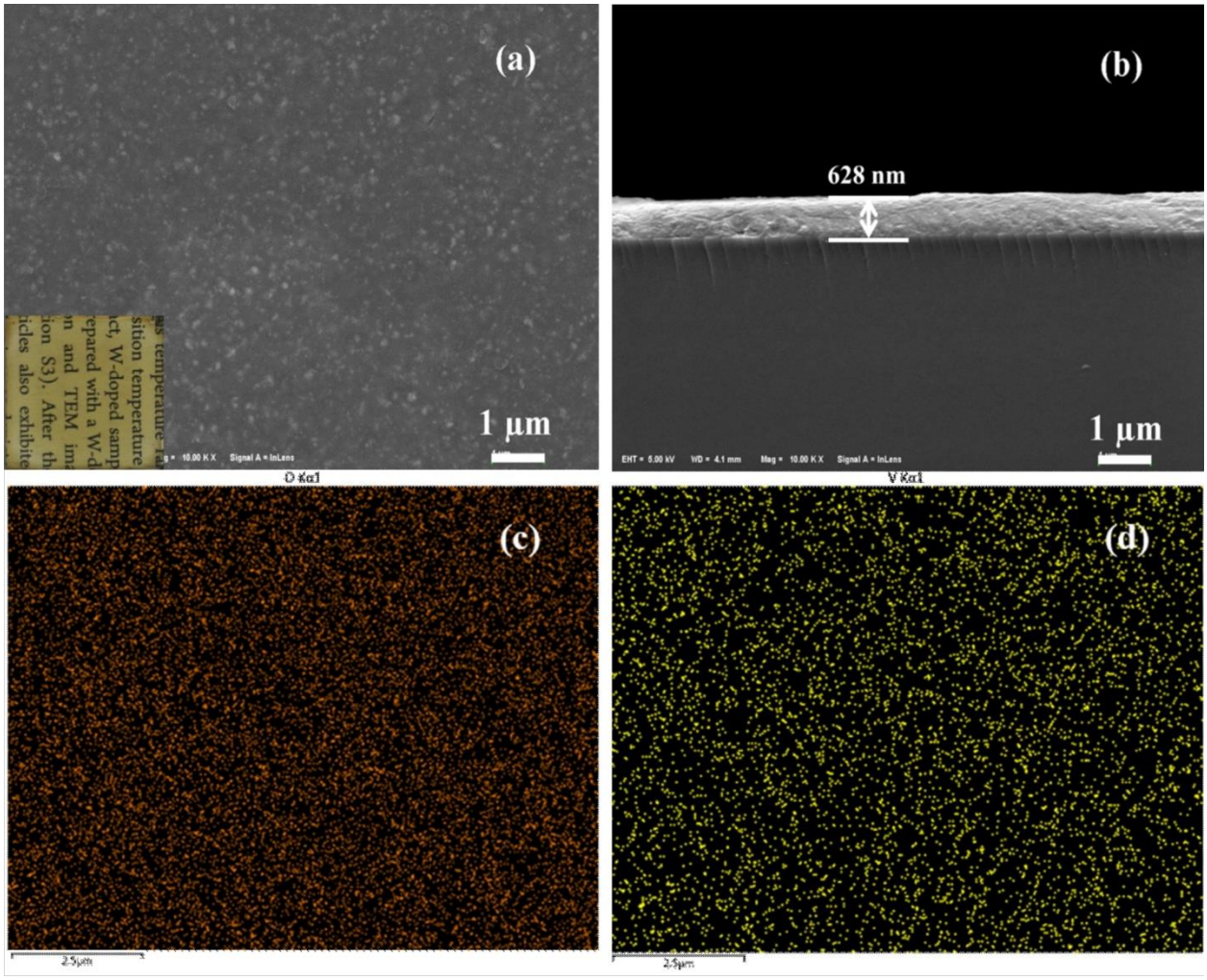

Fig. 5 (a) the surface (the inset shows the photograph (2.5*2.5 cm) of film on the glass), (b) the cross-section SEM images, (c) O element distribution and (d) V element distributions of the VO_2 based film prepared using the VO2 sample prepared from the Sample d produced at 180oC hydrothermal reaction temperature.

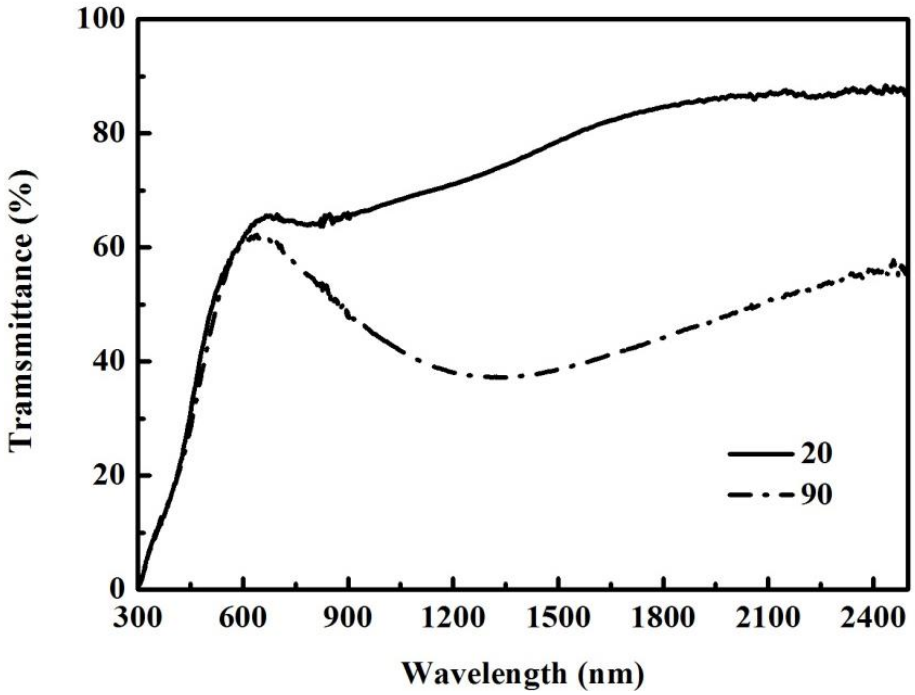

Fig. 6 Transmittance spectra of the films based on the VO_2 prepared using the VO2 sample prepared from the Sample d produced at 180oC hydrothermal reaction temperature.

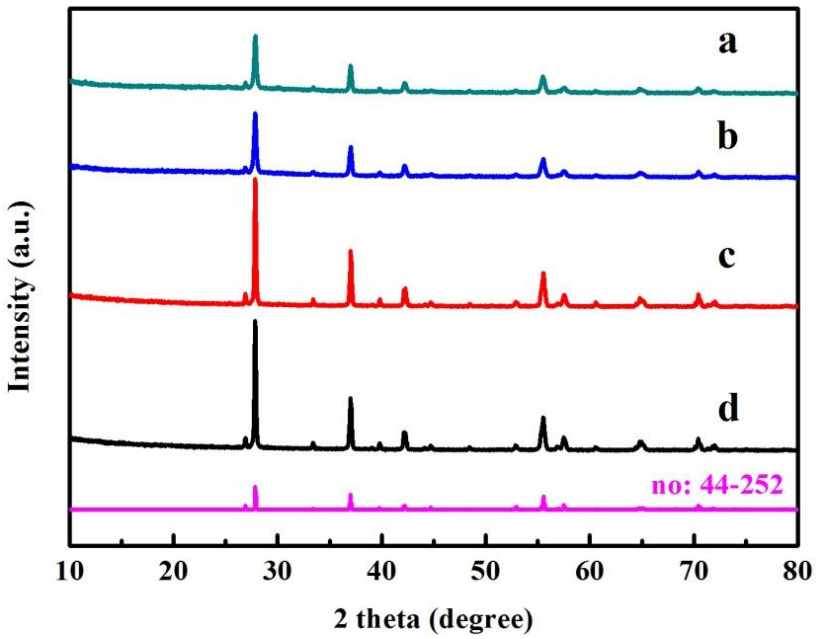

Fig. 7 The XRD patterns of the samples prepared at different temperatures (a-120 ℃, b-140 ℃, c-160 ℃, d-180 ℃). Note that these samples were subjected to drying, calcination to remove template and reduced in ammonium bicarbonate vapours at 450oC

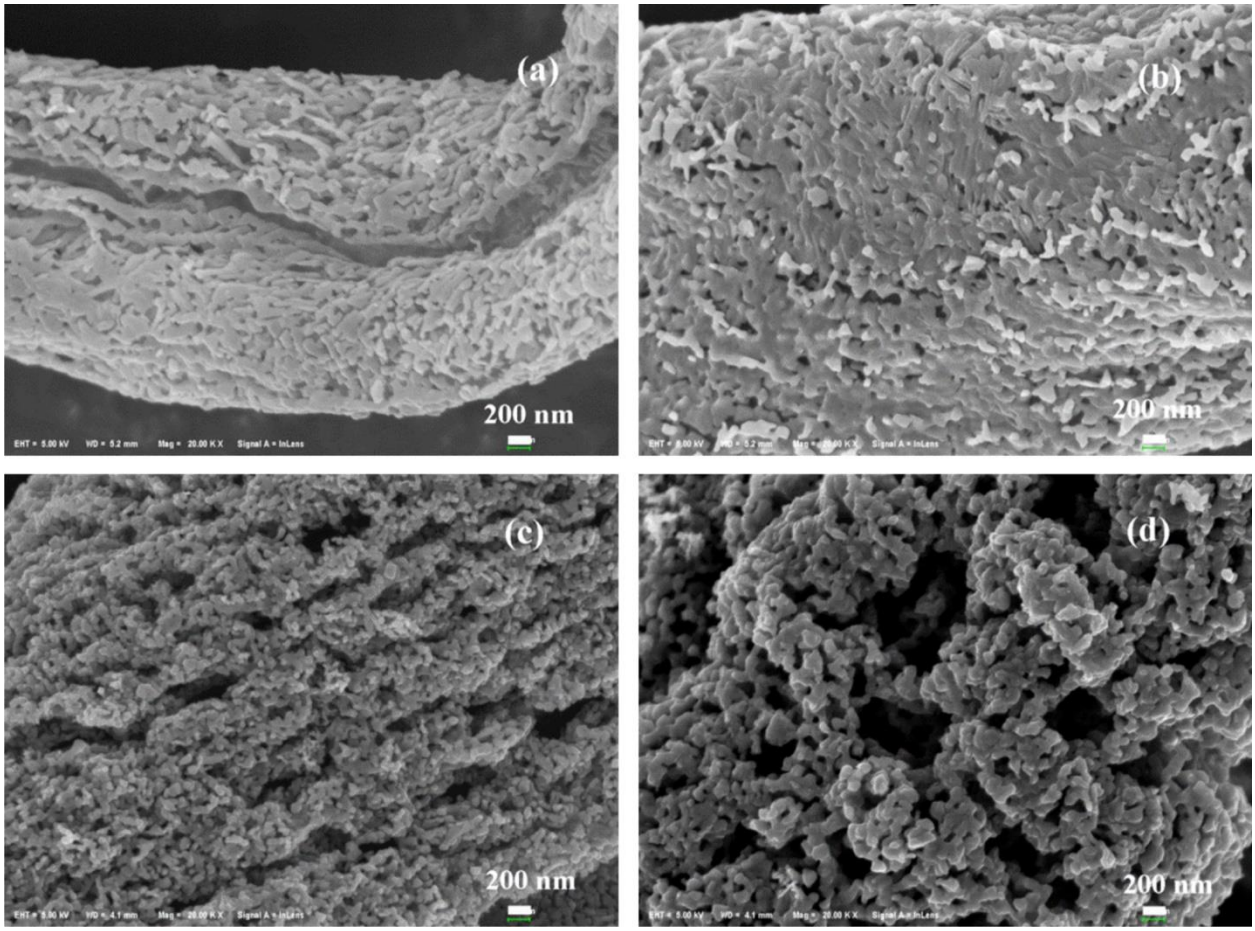

Fig. 8 SEM images of samples prepared at different temperatures (a) Sample a-120 ℃, (b) Sample b-140 ℃, (c) Sample c160 ℃ and (d) Sample d180 ℃. Note that these samples were subjected to drying, calcination to remove template and reduced in ammonium bicarbonate vapours at 450oC

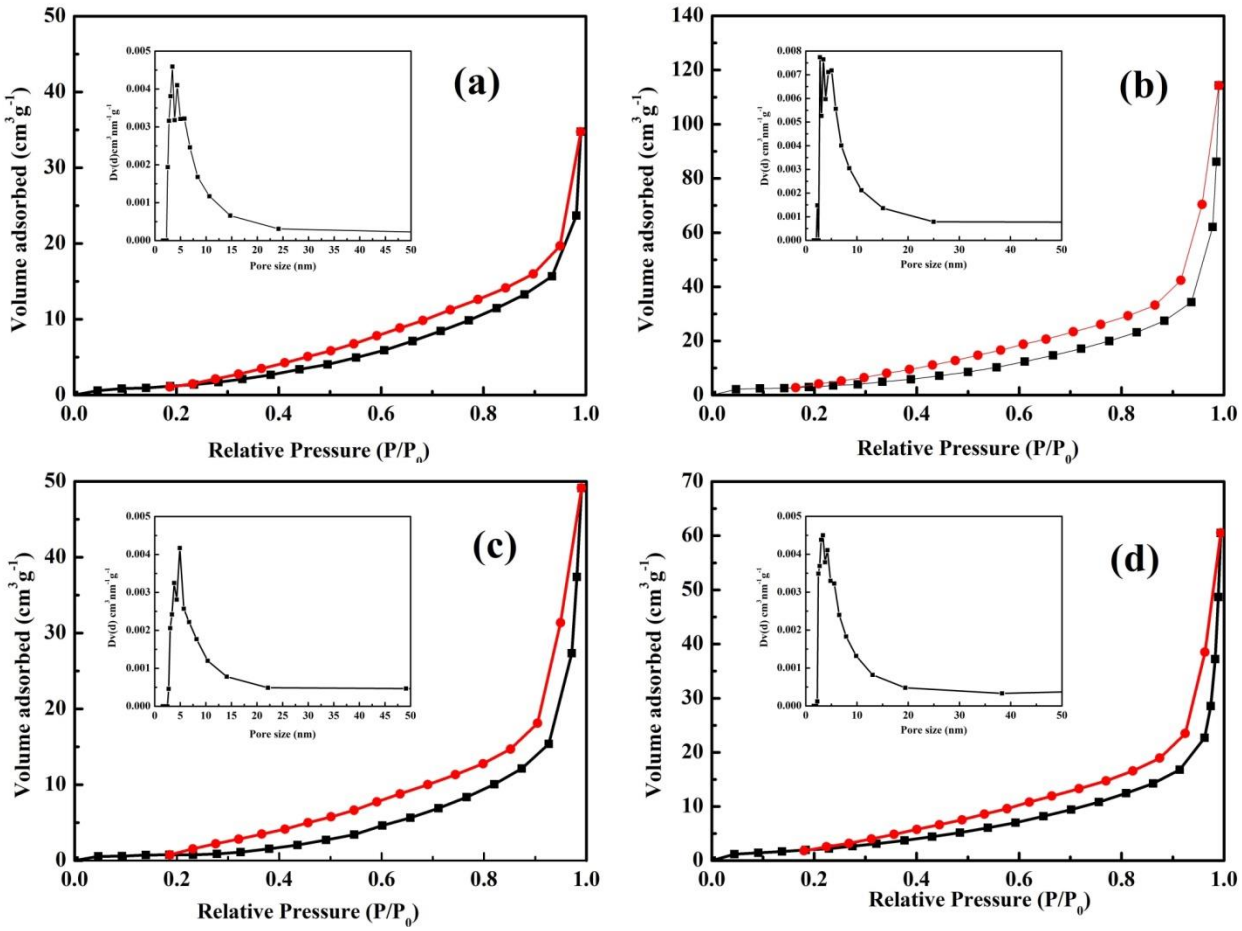

Fig. 9 N_2 adsorption/desorption curves and pore size distribution curves of Samples prepared at different temperatures (a-120 ℃, b-140 ℃, c-160 ℃, d-180 ℃). Note that these samples were subjected to drying, calcination to remove template and reduced in ammonium bicarbonate vapours at 450oC

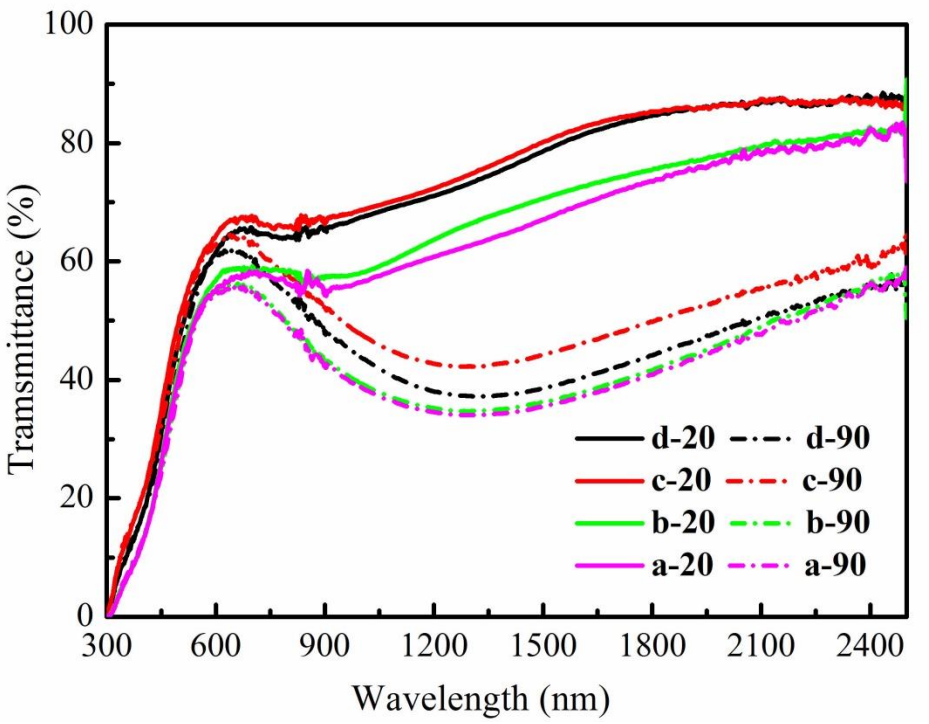

Fig. 10 Variable temperature UV/vis spectra of thin films of Samples prepared at different temperatures (a-120 ℃, b-140 ℃, c-160 ℃, d-180 ℃). Note that these samples were subjected to drying, calcination to remove template and reduced in ammonium bicarbonate vapours at 450oC. The spectra were obtained at 20 and 90 °C.

Table 1 The thermochromic properties of VO_2 composite films at different hydrothermal temperatures.

Sample	Temperatures (℃)*	Particle size (nm)#	mean pore size (nm)%	T_{lum} (%)&		ΔT_{sol} (%)&
				25 ℃	90 ℃	
Sample a	120	36.2	3.23	50.1	49.1	9.8
Sample b	140	36.3	5.05	51.3	49.7	10.7
Sample c	160	59.4	10.58	59.0	57.4	11.4
Sample d	180	60.7	3.78	56.0	54.3	12.9

* denotes the hydrothermal reaction temperature

Particle size estimated based on XRD data of the powder samples

% Pore size based on BET measurements of the powder samples

& Optical measurements reported here are from the PVP-VO2 composite films